

[advances.sciencemag.org/cgi/content/full/7/22/eabb9569/DC1](https://advances.sciencemag.org/cgi/content/full/7/22/eabb9569/DC1)

## Supplementary Materials for

### **Crowdsourced air temperatures contrast satellite measures of the urban heat island and its mechanisms**

Zander S. Venter\*, Tirthankar Chakraborty, Xuhui Lee

\*Corresponding author. Email: [zander.venter@nina.no](mailto:zander.venter@nina.no)

Published 26 May 2021, *Sci. Adv.* 7, eabb9569 (2021)

DOI: [10.1126/sciadv.abb9569](https://doi.org/10.1126/sciadv.abb9569)

#### **This PDF file includes:**

Tables S1 to S3  
Figs. S1 to S16

**Table S1. Random Forest model performance.**  $R^2$  and root mean square error (RMSE) values from the regression of observed on predicted local-scale ( $n = 5703$  stations) surface urban heat island (SUHI) and canopy UHI (CUHI) for all urban clusters ( $n = 342$ ) and a subset of clusters ( $n = 30$ ) which contained building height data. Performance statistics are derived using a validation dataset withheld from the Random Forest training. Mean values are reported  $\pm$  standard error.

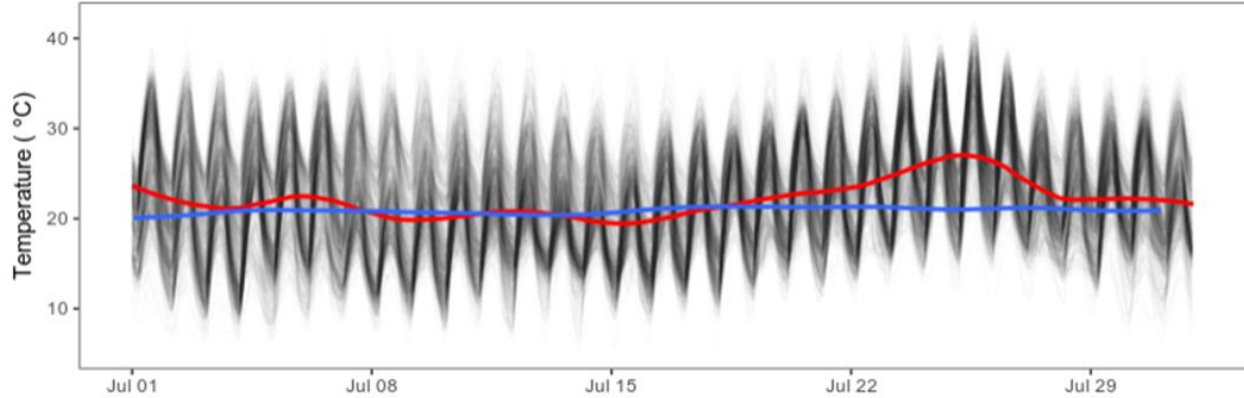
	Temperature source	Type	$R^2$		RMSE		
Subset Clusters	SUHI	Day	0.60	$\pm$ 0.002	1.56	$\pm$ 0.004	
		Night	0.54	$\pm$ 0.003	0.77	$\pm$ 0.003	
	CUHI	Day	0.06	$\pm$ 0.002	1.14	$\pm$ 0.003	
		Night	0.35	$\pm$ 0.003	0.93	$\pm$ 0.002	
All clusters	SUHI	Day	0.44	$\pm$ 0.003	1.73	$\pm$ 0.004	
		Night	0.38	$\pm$ 0.003	0.80	$\pm$ 0.001	
	CUHI	Day	0.15	$\pm$ 0.003	1.19	$\pm$ 0.003	
		Night	0.37	$\pm$ 0.002	0.95	$\pm$ 0.002	

**Table S2. Multiple linear regression model performance and variable importance.** Relative variable importance (%) produced from multiple linear regressions of local-scale (n = 5703 stations) surface urban heat island (SUHI) and canopy UHI (CUHI) on aerodynamic roughness and evapotranspiration for the subset of clusters (n = 30) with building height data. Separate models were produced for day and night time temperatures.

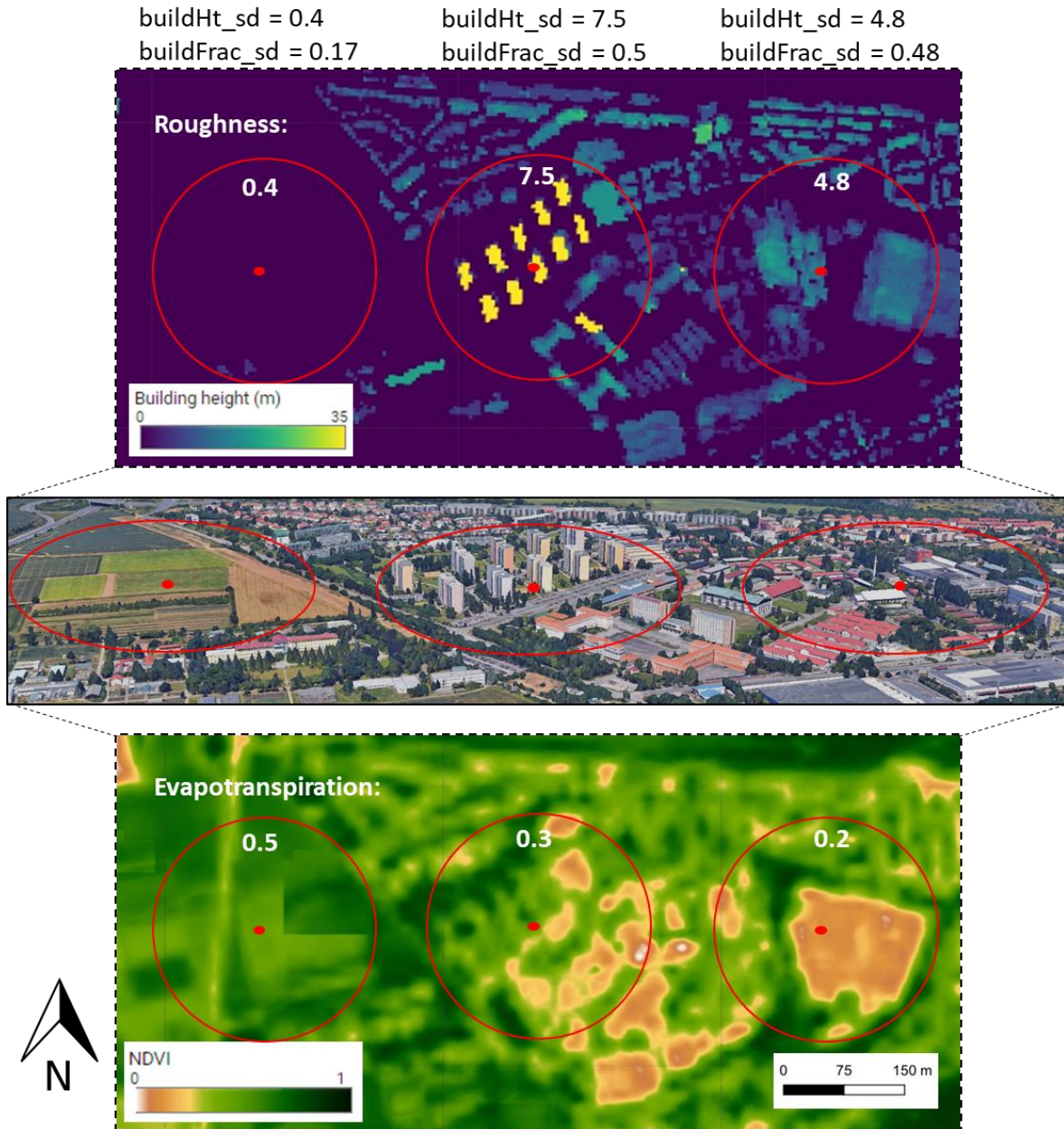
Temperature source	Type	Variable importance (%)		Model statistics	
		Roughness	Evapotranspiration	R <sup>2</sup>	F-statistic
SUHI	Day	3.3	96.7	0.276	1906
	Night	55.1	44.9	0.222	1424
CUHI	Day	13.3	86.7	0.009	46
	Night	40.7	59.3	0.205	1290

**Table S3. Predictor variables for Random Forest modelling of city-rural temperature differentials.** All variables were derived from gridded (raster) datasets which had different spatial resolutions. For CUHI models, mean data values were extracted for a range of buffer zones around each Netatmo station. For SUHI models, raster data were resampled to MODIS LST resolution and values extracted for each grid cell within urban clusters and their rural buffer zones.

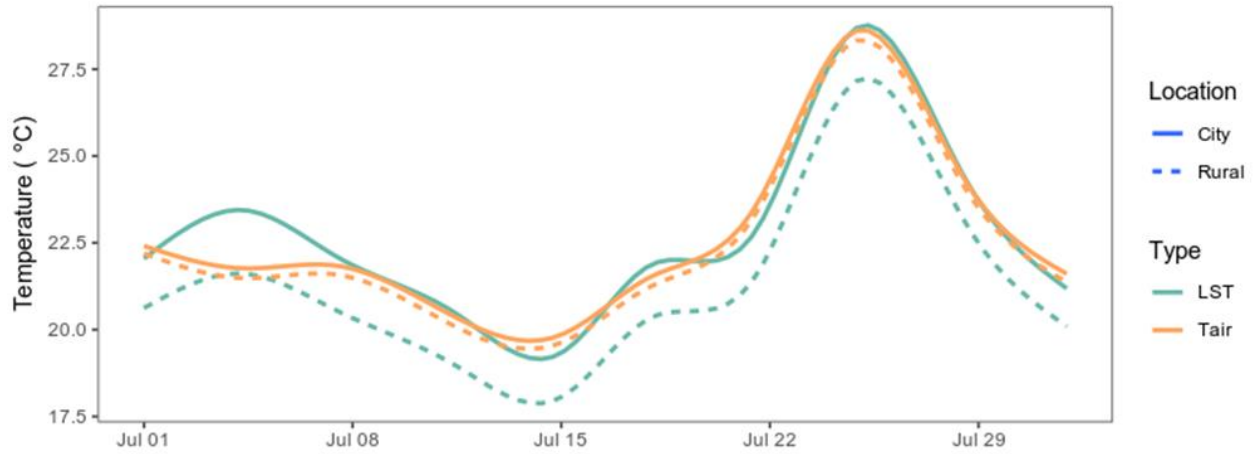
<b>Variable type</b>	<b>Variable Name</b>	<b>Resolution input data (m)</b>	<b>Description</b>
Land cover	ISA	100	Proportion of impervious surface area (%)
	Dist. Coast	500	Distance to coastline (km)
	Albedo	500	Mean black sky albedo MODIS
	NDVI	30	Normalized difference vegetation index
Terrain morphology	Elevation	30	Elevation above sea level (m)
	Slope	30	Terrain slope
	CHILI	90	Continuous heat-insolation load index
	TDIV	90	Topographic diversity index
	TPI	90	Topographic position index
City morphology	Building fraction	2.5	Fractional building cover
	Building height	10	Mean building height (m)
	Building height stdDev	10	Standard deviation in 100m2 mean building height



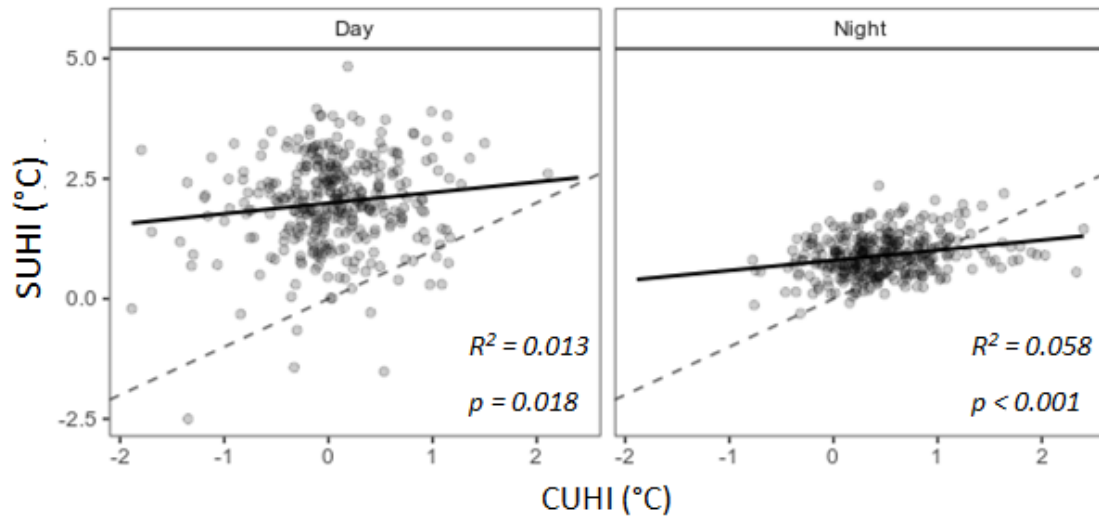
**Fig. S1. Hourly air temperatures from private weather stations over Europe during July 2019.** Each black line represents the hourly average across the available Netatmo stations within one of 342 urbans. A loess regression line across all cluster means is plotted in red. A 10-year (2009-2019) daily temperature mean is plotted in blue for reference using data from ERA5. We used the ERA5 fifth generation ECMWF atmospheric reanalysis of the global climate.



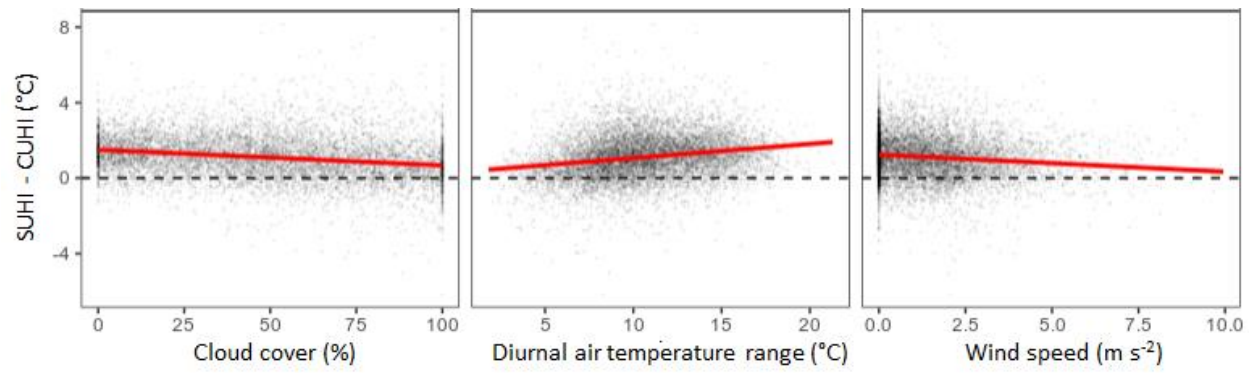
**Fig. S2. Illustration of aerodynamic roughness and evapotranspiration proxies.** An oblique angle view of a 2km wide urban-rural gradient in Prague, Czechia (center) shows a range of urban surface morphologies and vegetation cover. The hypothetical location of three weather stations and 250m buffer zones are overlain in red. The building height map (top) is used to calculate the standard deviation in building height within each buffer zone, as a proxy for aerodynamic roughness, and is indicated with white text. The normalized difference vegetation index (NDVI, bottom) is used as a proxy for evapotranspiration and the mean values within each buffer zone are indicated with white text. NDVI was derived from all available cloud-masked Landsat 8 Operational Land Imager surface reflectance scenes intersecting this area during July 2019.



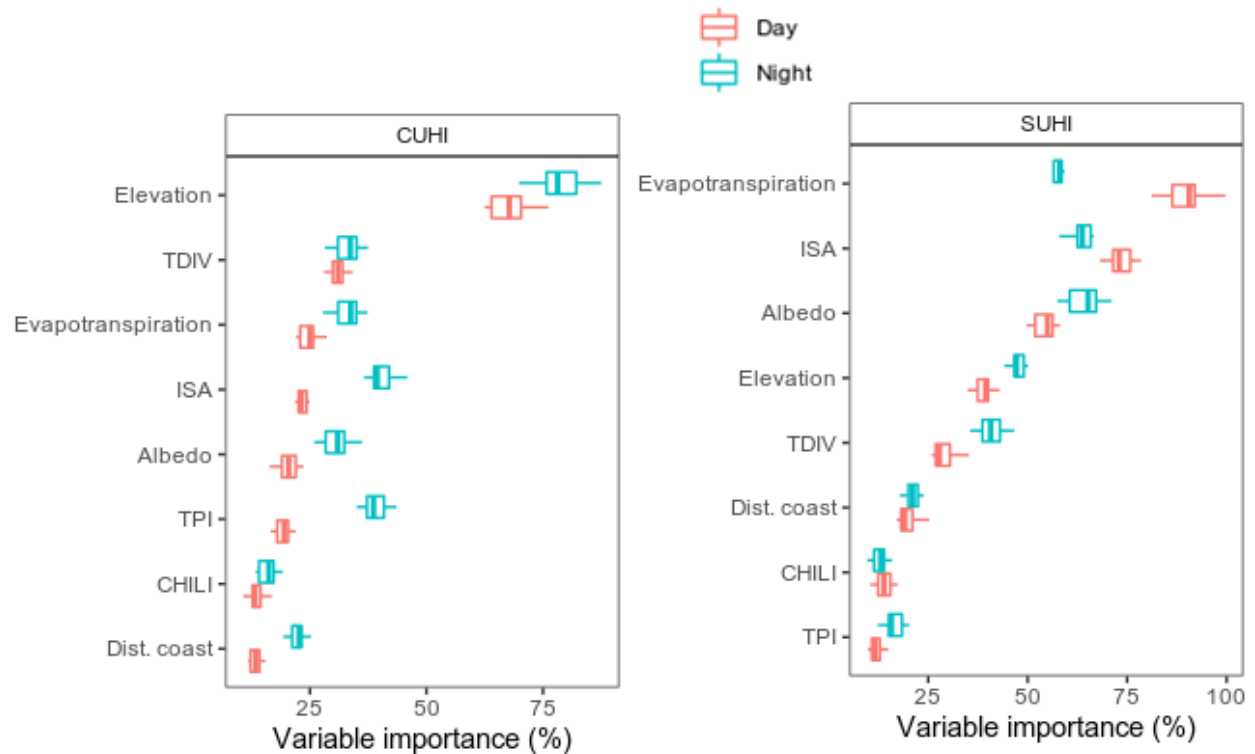
**Fig. S3. Mean urban and rural temperatures over Europe during July 2019.** Loess regression lines are fitted to mean city and rural buffer zone temperatures for all urban clusters in Europe. Separate lines are fitted for air temperatures ( $T_{air}$ ) from private weather stations and land surface temperatures (LST) from MODIS satellites.



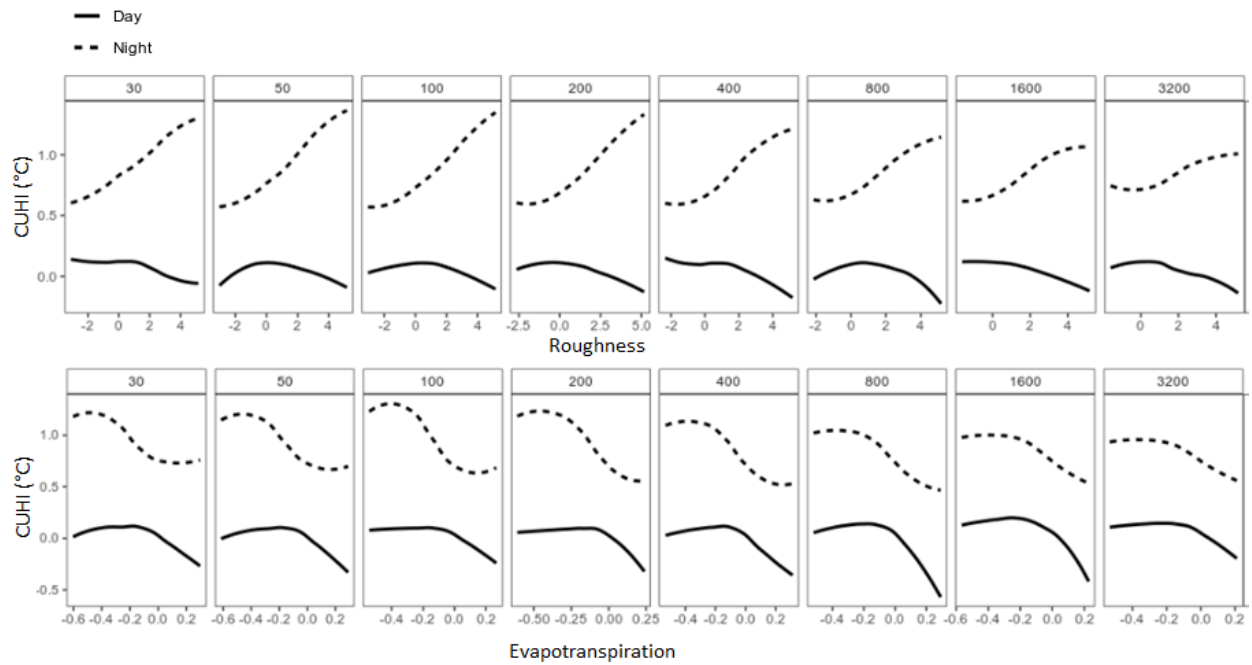
**Fig. S4. Surface-canopy urban heat island (UHI) intensity relationships.** Correlations between the mean of daytime and nighttime UHI intensities measured for urban clusters over Europe during July 2019. Linear regression lines are fitted in black with a 1:1 correlation line in dashes for reference.



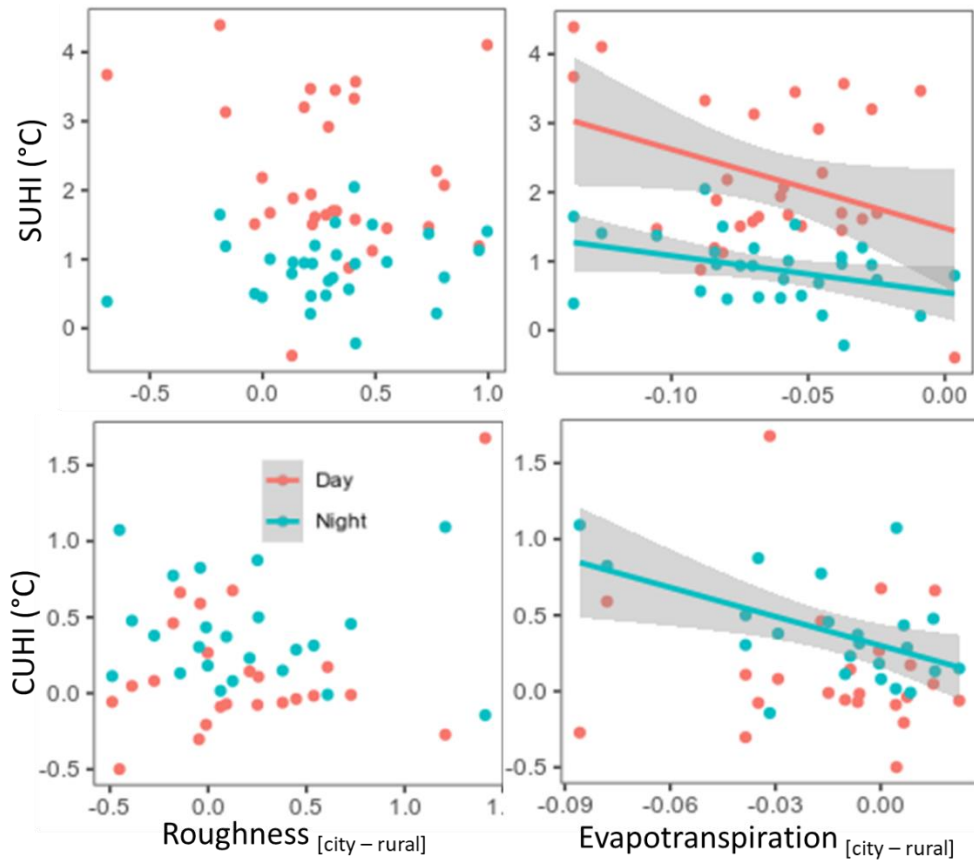
**Fig. S5. Effects of daily weather on SUHI-CUHI differentials.** Monthly time series of daily average SUHI-CUHI differentials for each urban cluster are regressed on average daily cloud cover, diurnal temperature range and wind speed. Linear regression line with 95% confidence intervals plotted with line and ribbon.



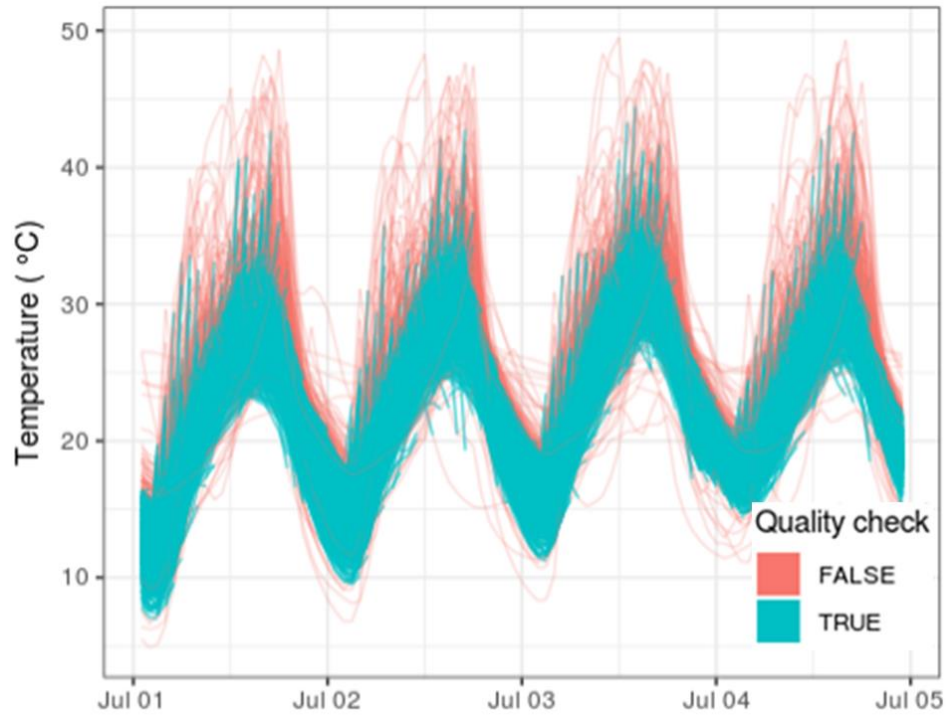
**Fig. S6. Variable importance for models explaining local-scale CUHI and SUHI over 342 urban clusters.** The variable importance scores for each predictor variable is expressed as the percentage increase in Random Forest model error when removing the corresponding predictor from the model. Importance scores are ordered from most to least important (top to bottom) for daytime UHI and are plotted with box-and-whisker plots reflecting the variation introduced by bootstrapping the random partitioning of training and testing data ( $n = 10$ ). Importance scores are plotted for models explaining the variance in local-scale SUHI and CUHI measured with satellite-derived land surface temperatures (LST) and private weather station air temperatures ( $T_{\text{air}}$ ), respectively. Models are further stratified into day time and night time UHI.



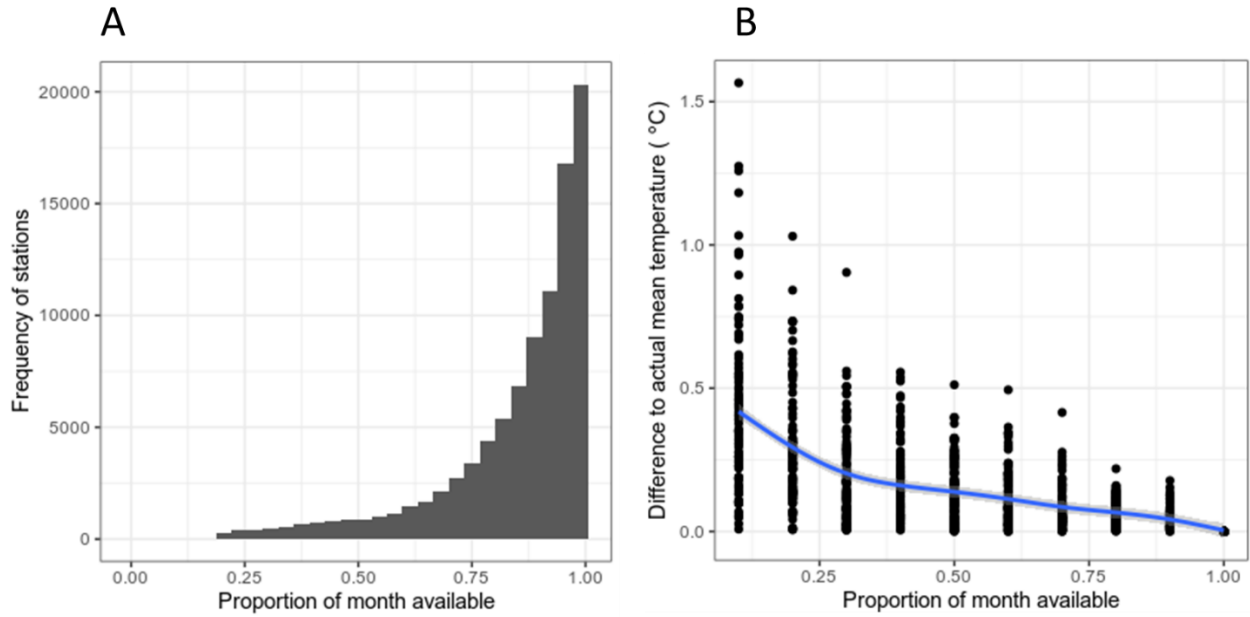
**Fig. S7. Effect of scale on the partial dependence of air temperature on aerodynamic roughness and evapotranspiration.** Separate Random Forest models were trained on data collected within varying buffer zone sizes (m) of each weather station and are faceted horizontally in the plot. The partial effect of roughness (top row) and evapotranspiration (bottom row) on air temperature differentials are plotted for day and night temperatures.



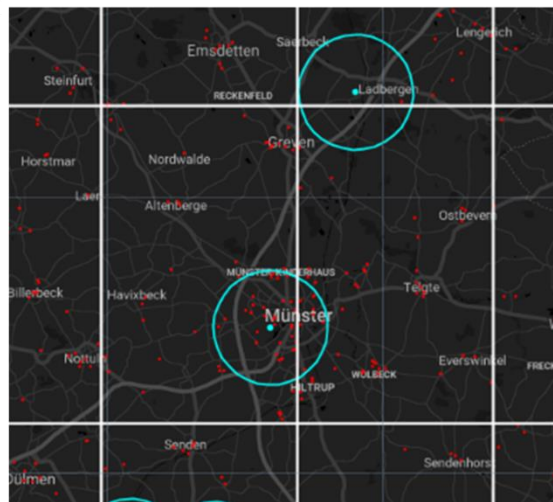
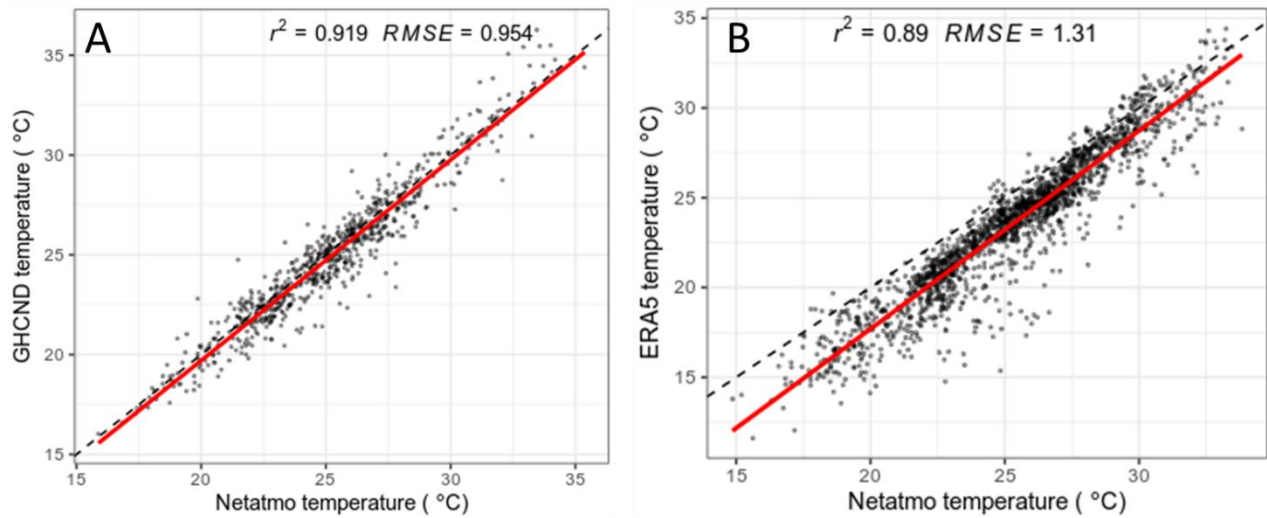
**Fig. S8. Associations between mean UHI and city-rural aerodynamic roughness and evapotranspiration differentials.** Mean daytime and nighttime CUHI and SUHI are regressed on mean city-rural differentials for roughness and evapotranspiration for a subset of urban clusters ( $n = 30$ ) with building height data. Each data point represents the value for one city and linear regression lines are fitted for significant ( $p < 0.05$ ) relationships tested by analysing the variance explained in multiple linear regression models.



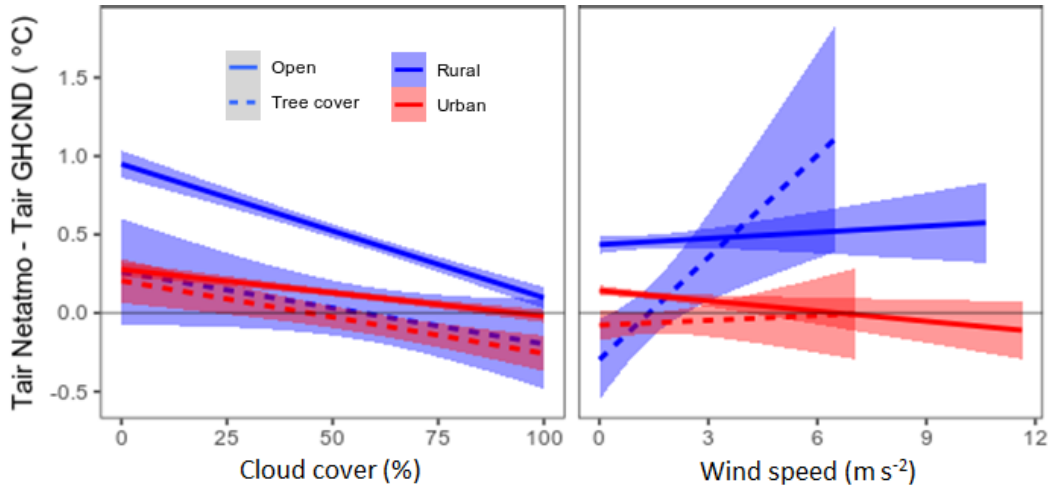
**Fig. S9. Quality assurance and cleaning of Netatmo weather station data.** A five-day time series for 503 stations in Oslo, Norway, is plotted to illustrate the performance of the quality assurance at removing outlying (“FALSE”)  $T_{\text{air}}$  values.



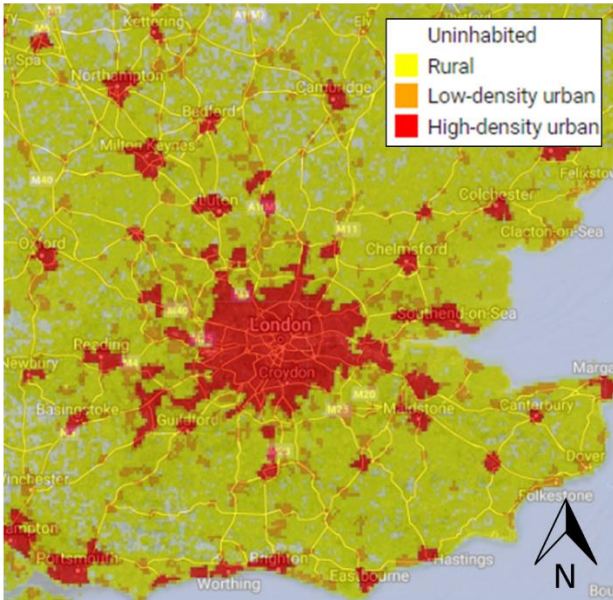
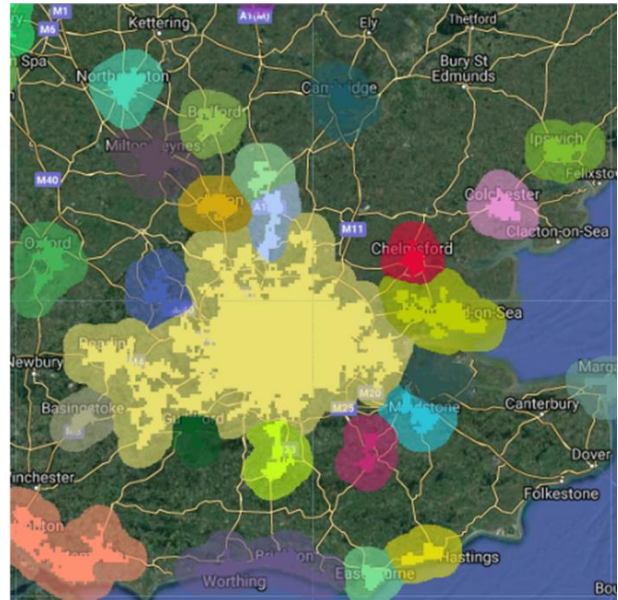
**Fig. S10. Temporal coverage of Netatmo weather stations.** The frequency distribution of proportional coverage for July 2019 Tair time series is plotted in A. A sensitivity test for 500 stations with full data coverage is shown in B. The absolute deviation from actual mean Tair is plotted for subsets of Tair readings with randomly removed data. A loess regression line is plotted in blue.



**Fig. S11. Validation of Netatmo weather station data.** Validation of monthly means of daily maximum  $T_{\text{air}}$  from Netatmo private weather stations. Validation against GHCND (A) and ERA5 (B) datasets are performed using spatial joins with Netatmo stations. The mean value for Netatmo stations within a 2km buffer of GHCND stations or ~20km ERA5 grid cell were used to compare with the GHCND and ERA5 readings, respectively (C). Linear regression lines are plotted in red with a dashed 1:1 line for reference.



**Fig. S12. Netatmo upward bias and cloud cover.** Daily Netatmo-GHCND differentials are regressed on percentage cloud cover. Cloud cover is relativized to monthly means. Linear regression lines and 95% confidence ribbons are plotted for stations in urban ( $n = 5535$ ) and rural ( $n = 1759$ ) zones.

**A****B**

**Fig. S13. Delineation of urban clusters over Europe.** The low- and high-density urban pixels of the Human Settlement Layer (A) were considered for urban clusters. These were grouped into objects based on connected pixels, filtered for those  $<40\text{km}^2$  and buffered by 10km using a focal mode kernel. Unique urban clusters are mapped with distinct colours in B. Urban cluster city and rural zones are differentiated by opaque and semi-transparent colouring, respectively. This image shows the greater London area in England.

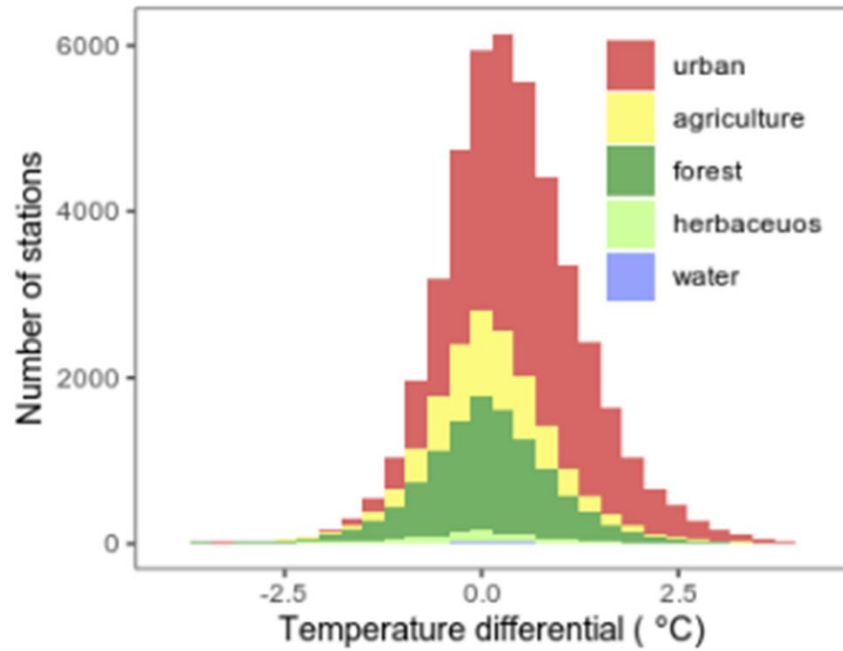


**Fig. S14. Netatmo station metadata.** Histogram showing the distribution of city-rural  $T_{air}$  differentials across land cover classes for all stations ( $n = 59810$ ) within 342 urban clusters and rural buffer zones included in the study.

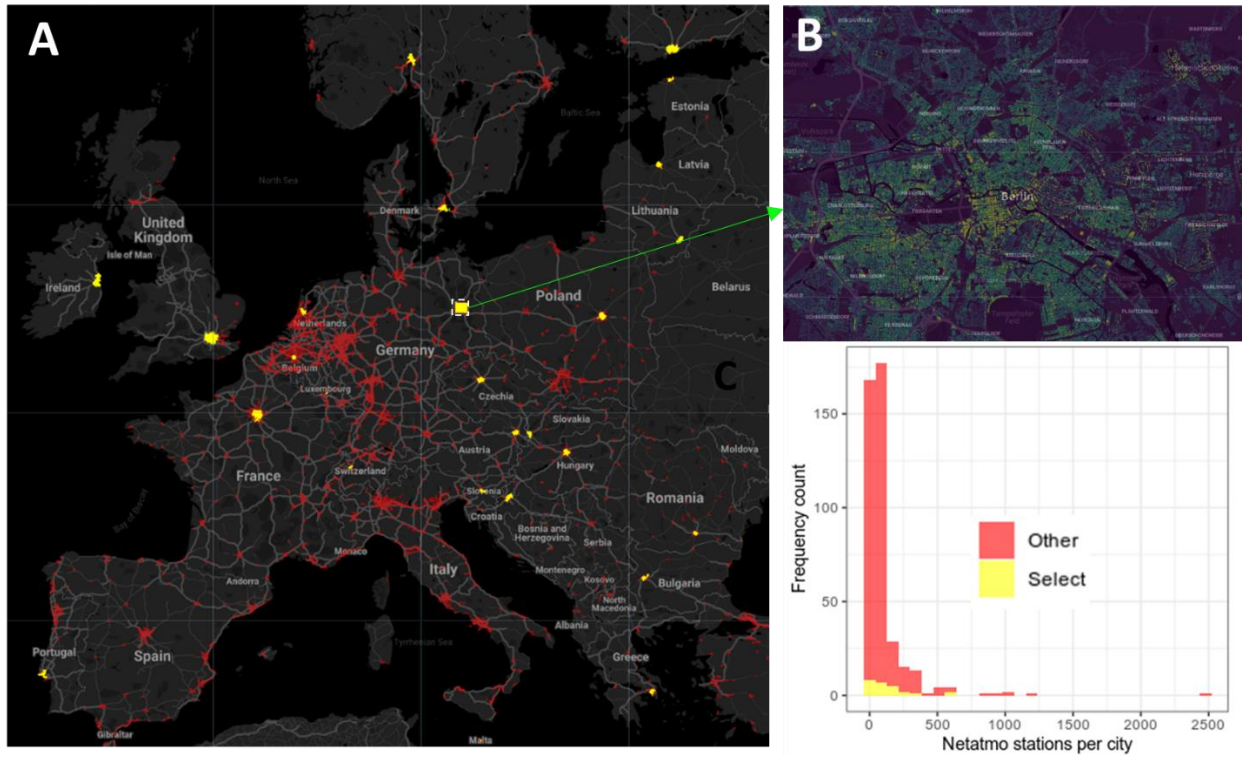


**Fig. S15. Distribution of urban clusters with building height data.** A subset of the 342 urban clusters (red in A) used for UHI calculation were used in the Random Forest modelling of city-rural temperature differentials. These 30 urban clusters (yellow in A) had building height data at 10m resolution (B) and contained 5703 of the Netatmo weather stations (C).

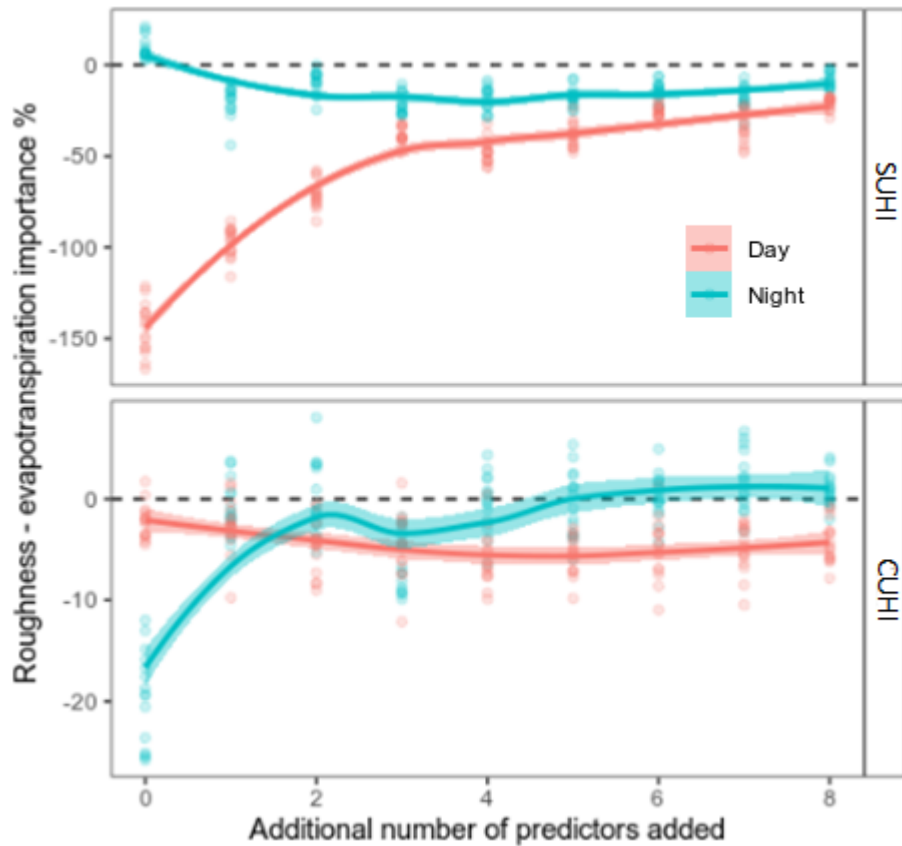


**Fig. S16. Effect of predictor variable number on aerodynamic roughness vs evapotranspiration importance scores.** The difference between variable importance scores (roughness subtract evapotranspiration) for day and night local-scale surface urban heat island (SUHI) and canopy UHI (CUHI) models are plotted (points) after iteratively adding predictor variables to the null model. The null model included only roughness and evapotranspiration as predictors. Loess regression lines are fitted with 95% confidence interval ribbons.